C. R. Mecanique 340 (2012) 526–535

Contents lists available at SciVerse ScienceDirect

Comptes Rendus Mecanique

www.sciencedirect.com

Analytical and innovative solutions for heat transfer problems involving phase change and interfaces

LB simulation of heat transfer in flow past a square unit of four isothermal cylinders

Javad Abolfazli Esfahani *, Ahmadreza Vasel-Be-Hagh

Department of Mechanical Engineering, Faculty of Engineering, Ferdowsi University of Mashhad, Mashhad 91775-1111, Iran

ARTICLE INFO

Article history:
Available online 15 May 2012

Keywords:
Thermal lattice Boltzmann
Low Reynolds number flow
Convection heat transfer
Flow past cylinders
In-line square configuration

ABSTRACT

The lattice Boltzmann method is applied to simulate heat transfer in flow past a square unit of four circular cylinders which its spacing ratio is fixed at $L/D = 2$. The cylinders are isothermal and also equal-diameter. The simulation is carried out at a fixed Prandtl number of 0.71, however, the Reynolds number takes three different values; $\mathrm{Re} = 80$, 120 and 200. The D2Q9 model is chosen to simulate fluid flow and the D2Q5 model is employed to simulate heat transfer. It is found that the predictions from the present simulation are excellently in accordance with results obtained from finite element solution of Navier–Stokes and energy equation.

1. Introduction

During last decades, flow and heat transfer around cylinder-like structures has become an active area of research due to its great practical engineering applications including tubular heat exchangers. In this way, in parallel to the advances of experimental techniques for the flow and heat transfer characteristics measuring, several computational techniques have been developed to investigate this pragmatic issue. One of these techniques is the lattice Boltzmann (LB) method which, unlike classical CFD solvers, is on the basis of the Boltzmann equation. Due to its mesoscopic nature, the LB method has many exceptional qualities involving high computational performance, not having mesh tangling and easy implements for complex fluid–solid boundary conditions which have made it highly appropriate for fluid dynamics and heat transfer analyses of the flow around structures including any number of cylinders with any cross-section shape and arrangement. Accordingly, many researchers have used this method to study the fluid mechanics of the flow around structures including one [1–4], two [5–8] and recently more than two cylinders [9,10]. In contrast to this wide usage, only a few researchers have applied the LB approach to study the heat transfer of the flow around cylindrical structures which are reviewed comprehensively in the following part.

In the context of the LB method application in heat transfer study of such flow, for the first time in 2006, Chen et al. [11] analyzed the velocity and temperature fields of a low Reynolds number backward-facing step flow with insertion of a single circular cylinder. Reynolds number range of this simulation was limited to a maximum value of 200. Then in 2008, Zu et al. [12] developed a boundary treatment for curved and moving boundaries. They used a multi-distribution function thermal LB model to simulate the flow and heat transfer around a rotating circular cylinder. This simulation was conducted at Reynolds numbers of 200, 500 and 1000, and the Prandtl number was set at 0.5 and 1.0. Following that, Yan et al. [13] studied flow past a rotating isothermal cylinder with heat transfer using the LB method. This simulation was done at Reynolds number of 200, 218, 500 and 1000. Also four different Prandtl numbers were applied; $\mathrm{Pr} = 0.1$, 0.5, 0.71 and 1. Later in 2009, firstly Yen et al. [14] analyzed the velocity and temperature fields of a low Reynolds number backward-facing

* Corresponding author.
E-mail addresses: abolfazl@um.ac.ir, Jaesfahani@gmail.com (J.A. Esfahani).

1631-0721/$ – see front matter
http://dx.doi.org/10.1016/j.crme.2012.03.011

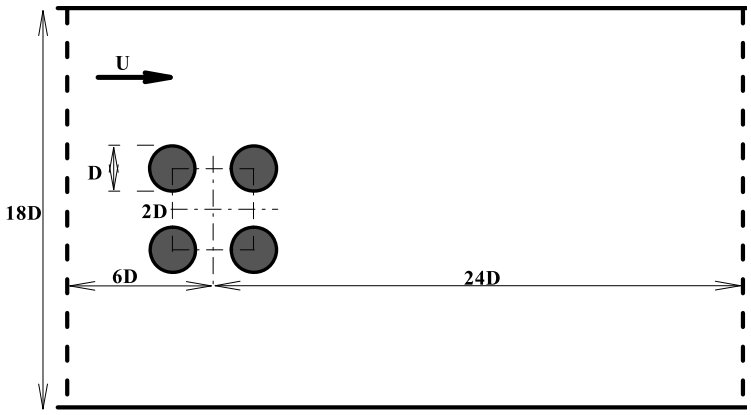

Fig. 1. Schematic diagram of the computational domain.

step flow with insertion of a circular cylinder. The simulation was carried out for two different cases; stationary and rotating cylinder. Reynolds number range of this research was limited to a maximum value of 200. Then, Djenidi et al. [15] used the LB method to simulate three-dimensional flow past a heated square cylinder at a Reynolds number of 200 and a Prandtl number of 0.7. After that, Yang et al. [16] studied the enhancement of heat transfer by putting cylindrical pillars inside a channel flow. In that research, the field synergy principle was applied to demonstrate the fact that while the interruption within the fluid increased, the synergistic level between the velocity field and temperature gradient field raised. Lastly, Moussaoui et al. [17] coupled a multiple-relaxation-time LB equation with the finite difference method to simulate laminar incompressible fluid flow and heat transfer in a plane channel with two square blocks located at arbitrary positions. In 2010, first of all, Kang et al. [18] conducted an LB simulation of flow and heat transfer around a single circular cylinder at two different Reynolds numbers, $\mathrm{Re} = 0.8$ and 34. In the meanwhile, Ghasemi et al. [19] used thermal Finite-Volume LB method to simulate the fluid flow around a circular cylinder inserted within a backward-facing step. They investigated the temperature field at Pr number of 0.7 and six different Reynolds numbers ranging from 10 to 485. Finally, Moussaoui et al. [20] coupled the LB method with the finite difference method to simulate fluid flow and heat transfer in a horizontal channel obstructed by an inclined square cylinder with inclination angle of 45°. At first, they used the multiple-relaxation-time LB method to compute the fluid flow and used its results to solve the energy equation by a finite difference method. This research was done at Pr number of 0.7 and different Reynolds numbers up to 300.

Here the LB method is used to simulate heat transfer of the flow around a square unit of four isothermal circular cylinders to compare its results with results obtained by the finite element solution of Navier–Stokes and energy equation. The simulation is conducted at Prandtl number of 0.71 and three different Reynolds numbers; $\mathrm{Re} = 80$, 120 and 200. At first, the initial setup of the simulation is described. Then, a summary of mathematical model and boundary conditions which are employed in the simulation is prepared. Finally, the results of the simulation are presented in three forms; isotherms through the whole domain to investigate the temperature field pattern and its time evolution, temperature contours in the near vicinity of the cylinders to study the thermal shear layer, local and also mean Nusselt number to compare the rate of heat transfer at different points of the isothermal square unit.

2. Initial setup

The schematic diagram of the computational domain is shown in Fig. 1. As can be seen the cylinders are arranged in the in-line square configuration. The mentioned square unit is mounted inside a channel which is sufficiently wide in a way that its walls exert no measurable effect on the flow field characteristics. Moreover, the cylinders are assumed to be too long so that the ends effects are neglected.

Parameters D and L indicate cylinders diameter and the distance between their centers respectively. The ratio L/D is called spacing ratio which is fixed at $L/D = 2$ within the simulation. The channel is $18D$ in width so the shortest distance from each cylinder surface to the walls is $7.5D$ which in comparison with the chosen spacing ratio ($L/D = 2$) is long enough to eliminate the walls effects from the flow pattern around and behind the cylinders. Additionally, the area has an overall length of $30D$ which cylinders are set up at a mean distance of $6D$ down the inlet location. So the downstream area is extended $24D$ from the center of the square unit of cylinders. In this simulation, three different lattices were adopted on the computational domain on the basis of Reynolds number. These mentioned lattices contain 288×480, 432×720 and 720×1200 regular quads for the cases $\mathrm{Re} = 80$, 120 and 200 respectively. The temperature of the walls (T_w) is equal to the temperature of the incoming fluid (T_∞) which is constant during the computation. As well, the temperature of the cylinders surfaces (T_s) is assumed to be constant, however, higher than the incoming fluid temperature. In the current simulation, (T_∞) and (T_s) are chosen to be 1.00 and 2.00 respectively.

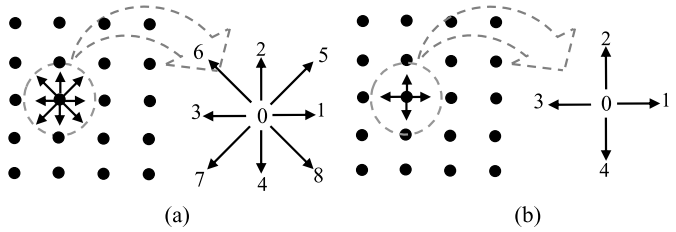

Fig. 2. (a): The two-dimensional nine-direction lattice called D2Q9. (b): The two-dimensional five-direction lattice called D2Q5.

3. Mathematical model

In this research the two-dimensional nine-direction D2Q9 and the two-dimensional five-direction D2Q5 models are applied to simulate fluid flow and heat transfer respectively. These models are presented in Fig. 2.

The D2Q9 lattice allows particles move only in 8 specific directions ($k = 1, \ldots, 8$) or rest at their place ($k = 0$). However, the D2Q5 lattice provides only 4 directions ($i = 1, \ldots, 4$) for the temperature distribution. In the following section the strategy formulation for these models is briefly described and the boundary conditions which are employed in this study are presented.

3.1. Governing equations

According to the models described in Fig. 2, the hydrodynamic and thermal LB equations with BGK approximation take the following forms, respectively:

$$f_k(x + e_k \cdot \Delta t, t + \Delta t) - f_k(x, t) = -\frac{1}{\tau_F}\left(f_k(x, t) - f_k^{\mathrm{eq}}(x, t)\right) \tag{1a}$$

$$g_i(x + c_i \cdot \Delta t, t + \Delta t) - g_i(x, t) = -\frac{1}{\tau_T}\left(g_i(x, t) - g_i^{\mathrm{eq}}(x, t)\right) \tag{1b}$$

where τ_F and τ_T are the relaxation times for the momentum and the temperature equations. In Eqs. (1a) and (1b) the equilibrium particle distribution function $f_k^{\mathrm{eq}}(x, t)$ and the equilibrium temperature distribution function $g_k^{\mathrm{eq}}(x, t)$ are given by the following equations:

$$f_k^{\mathrm{eq}}(x, t) = w_k \cdot \rho(x) \cdot \left[1 + 3\frac{\mathbf{e}_k \cdot u}{c^2} + \frac{9}{2}\frac{(\mathbf{e}_k \cdot u)^2}{c^4} - \frac{3}{2}\frac{u^2}{c^2}\right] \tag{2a}$$

$$g_i^{\mathrm{eq}}(x, t) = w_i \cdot T(x) \cdot \left[1 + 3\frac{\mathbf{c}_i \cdot u}{c^2}\right] \tag{2b}$$

In these equations c, ρ, u and T are respectively the lattice constant which is equal to 1 lu/ts, the fluid macroscopic density, velocity and temperature which all are in lattice units. Also w_k and w_i are the weight coefficients of permissible moving directions of the nine-direction and five-direction lattices described in Fig. 2 which take the following magnitude

$$w_k = \begin{cases} \frac{4}{9}, & k = 0 \\ \frac{1}{9}, & k = 1, 2, 3, 4 \\ \frac{1}{36}, & k = 5, 6, 7, 8 \end{cases} \tag{3a}$$

$$w_i = \begin{cases} \frac{1}{3}, & i = 0 \\ \frac{1}{6}, & i = 1, 2, 3, 4 \end{cases} \tag{3b}$$

The vectors $\mathbf{e}_k$ and $\mathbf{c}_i$ are unit vectors which represent the kth and ith directions respectively and take the following forms

$$\begin{cases} \mathbf{e}_k = 0, & k = 0 \\ \mathbf{e}_k = \left(\cos\left(\frac{\pi}{2}(k-1)\right), \sin\left(\frac{\pi}{2}(k-1)\right)\right), & k = 1, 2, 3, 4 \\ \mathbf{e}_k = \sqrt{2} \times \left(\cos\left(\frac{\pi}{2}\left(k - \frac{9}{2}\right)\right), \sin\left(\frac{\pi}{2}\left(k - \frac{9}{2}\right)\right)\right), & k = 5, 6, 7, 8 \end{cases} \tag{4a}$$

$$\begin{cases} \mathbf{c}_i = 0, & i = 0 \\ \mathbf{c}_i = \left(\cos\left(\frac{\pi}{2}(k-1)\right), \sin\left(\frac{\pi}{2}(k-1)\right)\right), & i = 1, 2, 3, 4 \end{cases} \tag{4b}$$

The LB equations (Eqs. (1a) and (1b)) can be solved through whole domain by implementing proper boundary conditions. By solving these equations, the single particle distribution function $f_k(x,t)$ and the temperature distribution function $g_i(x,t)$ will be known at each site of the lattice for all directions. The macroscopic quantities are then obtained in lattice units through moment integrations of the distribution function

$$\rho = \sum_{k=0}^{8} f_k \tag{5}$$

$$u = \frac{1}{\rho}\sum_{k=0}^{8} f_k \cdot e_k \tag{6}$$

$$T = \sum_{k=0}^{8} g_i \tag{7}$$

Obtaining the lattice density is equal to obtaining the lattice pressure since there is an equation of state that relates them directly. For the single component D2Q9 model this equation is simply [21]

$$P = c_s^2 \cdot \rho \tag{8}$$

in which c_s is the speed of sound in this model and has a close relation to lattice constant c which is given by

$$c_s = \frac{c}{\sqrt{3}} \tag{9}$$

By defining the shear viscosity and thermal diffusivity through the following equations [22]:

$$\nu = \frac{c^2}{3}\left(\tau_F - \frac{1}{2}\right) \tag{10}$$

$$\alpha = \frac{c^2}{3}\left(\tau_T - \frac{1}{2}\right) \tag{11}$$

the Navier–Stokes and energy equations can be derived from Eqs. (1a) and (1b). Accordingly, the Prandtl number, local Nusselt number and surface-averaged Nusselt number are calculated by the following equations:

$$\mathrm{Pr} = \frac{\nu}{\alpha} = \frac{\tau_F - \frac{1}{2}}{\tau_T - \frac{1}{2}} \tag{12}$$

$$\mathrm{Nu} = -\left(\frac{\mathrm{d}T}{\mathrm{d}n}\right)_{\mathrm{wall}} \tag{13}$$

$$\mathrm{Nu}_{\mathrm{s\text{-}ave}} = \frac{1}{2\pi}\int_0^{2\pi} \mathrm{Nu}\cdot \mathrm{d}\theta \tag{14}$$

where $\vec{n}$ denotes the local normal direction of the cylinders surface.

3.2. Hydrodynamic boundary conditions

In this study, three kinds of hydrodynamic boundary conditions are applied: bounce back condition is handled on the surface of the cylinders and the channel walls to obtain no slip boundary condition, constant velocity and constant pressure conditions are set at inlet and outlet boundaries respectively. The bounce back scheme which is used here is on the basis of the extrapolation method proposed by Guo et al. [23].

According to Fig. 3 the fraction of the intersected link, Δ, is defined as:

$$\Delta = \frac{|x_f - x_b|}{|x_f - x_w|} \tag{15}$$

In this definition, indices f, b and w indicate fluid, boundary and wall respectively. Moreover, it is clearly understood that to compute $f_i(x_f, t+\Delta t)$ the distribution function at wall $\widetilde{f}_i(x_w)$ is needed. The main idea of this method is decomposing this function into two parts: the equilibrium $f_i^{\mathrm{eq}}(x_w)$ and the non-equilibrium $f_i^{\mathrm{neq}}(x_w)$ parts. The equilibrium part $f_i^{\mathrm{eq}}(x_w)$ part is defined by

$$\overline{f}_i^{\mathrm{eq}}(x_w,t) = w_i \cdot \left[\overline{\rho}_w + \rho_0\left(3\frac{e_k\cdot\overline{u}_w}{c^2} + \frac{9}{2}\frac{(e_k\cdot\overline{u}_w)^2}{c^4} - \frac{3}{2}\frac{\overline{u}_w^2}{c^2}\right)\right] \tag{16}$$

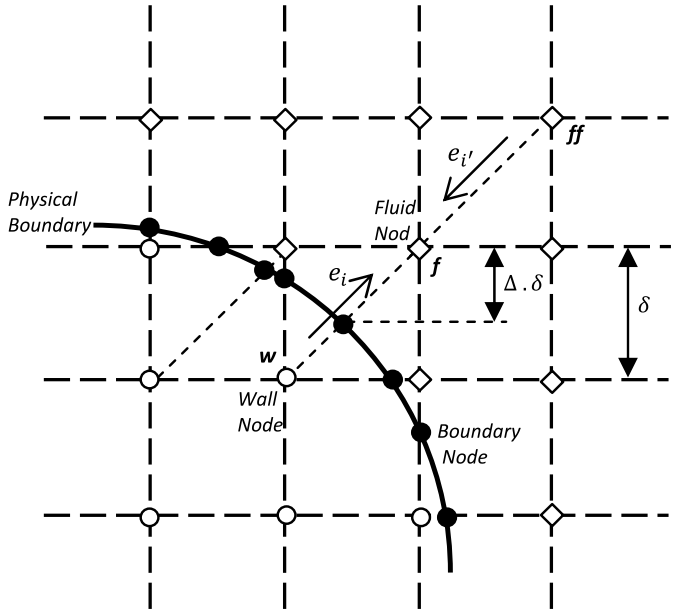

Fig. 3. Curved boundary of the cylinders and the lattice nodes.

where $\overline{\rho}_w$ is approximately equal to $\rho(x_f)$ and $\overline{u}_w$ is calculated by

$$\overline{u}_w = \begin{cases} \frac{u_b+(\Delta-1)u_f}{\Delta+1} & \text{for } \Delta \geqslant 0.75 \\ \frac{2u_b+(\Delta-1)u_{ff}}{\Delta+1} & \text{for } \Delta < 0.75 \end{cases} \tag{17}$$

in which $u_f = u(x_f)$, $u_{ff} = u(x_{ff})$ and the $u_b = u(x_b)$ is the boundary velocity which in the current study is assumed to be zero. The non-equilibrium part $f_i^{\text{neq}}(x_w)$ is

$$f_i^{\text{neq}}(x_w, t) = \begin{cases} f_i^{\text{neq}}(x_f) & \text{for } \Delta \geqslant 0.75 \\ \Delta \cdot f_i^{\text{neq}}(x_f) + (1-\Delta) f_i^{\text{neq}}(x_{ff}) & \text{for } \Delta < 0.75 \end{cases} \tag{18}$$

So $\widetilde{f}_i(x_w)$ is calculated as follows:

$$\widetilde{f}_i(x_w, t) = \overline{f}_i^{\text{eq}}(x_w, t) + \left(1 - \tau^{-1}\right) f_i^{\text{neq}}(x_w, t) \tag{19}$$

Finally, the following equation finishes the streaming step of the fluid node x_f:

$$f_i(x_f, t + \Delta t) = \widetilde{f}_i(x_w, t) \tag{20}$$

Fig. 4 shows unknown distribution functions at inlet and outlet boundaries. By implementing constant velocity and constant pressure boundary conditions, these unknown parameters will be related to those which are known from neighboring sites. In the current study, these boundary conditions have been applied in the same way which was proposed by Zou and He [24]. Here only the results are presented.

At the inlet boundary

$$\rho = \frac{(f_0 + f_1 + f_3) + 2 \times (f_3 + f_7 + f_6)}{1 - u_0} \tag{21}$$

$$f_1 = f_3 + \frac{2}{3}\rho \cdot u_0 \tag{22}$$

$$f_5 = f_7 + \frac{1}{6}\rho \cdot u_0 - \frac{1}{2}(f_2 - f_4) \tag{23}$$

$$f_8 = f_6 + \frac{1}{6}\rho \cdot u_0 - \frac{1}{2}(f_4 - f_2) \tag{24}$$

and at outlet boundary

$$u = -1 + \frac{(f_0 + f_2 + f_4) + 2 \times (f_1 + f_5 + f_8)}{\rho_0} \tag{25}$$

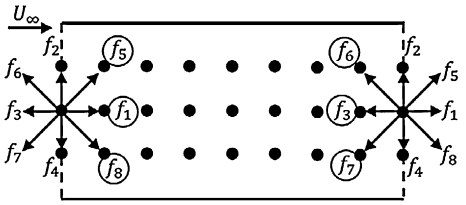

Fig. 4. Unknown distribution functions at the inlet and outlet boundaries. Circulated ones are unknown, others are known from neighbor sites through streaming process.

$$f_3 = f_1 - \frac{2}{3}\rho_0 \cdot u \tag{26}$$

$$f_6 = f_8 - \frac{1}{6}\rho_0 \cdot u + \frac{1}{2}(f_4 - f_2) \tag{27}$$

$$f_7 = f_5 - \frac{1}{6}\rho_0 \cdot u + \frac{1}{2}(f_2 - f_4) \tag{28}$$

where u_0 and $\rho_0/3$ are inlet velocity and outlet pressure, respectively. See Fig. 4.

3.3. Thermal boundary conditions

According to Fig. 3, at the node f the temperature distribution function at the direction i', $g_{i'}$, is known through the streaming process during the previous time step. However, the temperature distribution function at the direction i, g_i, is unknown because the g_i is coming from an inactive node (node w). This unknown parameter must be found in a way that satisfies the following equation:

$$g_i^{\text{neq}} - e_i^2 f_i^{\text{neq}} = -\left(g_{i'}^{\text{neq}} - e_{i'}^2 f_{i'}^{\text{neq}}\right) \tag{29}$$

To set out the constant temperature at the wall nodes, the g^{eq} must be calculated on the basis of the wall temperature, accordingly

$$\begin{aligned} g_i(x_f, t+\Delta t) = {} & (ex_i \times ex_i + ey_i \times ey_i) \times \left(f_i(x_f, t+\Delta t) - f_i^{\text{eq}}(x_f, t+\Delta t)\right) \\ & + (ex_{i'} \times ex_{i'} + ey_{i'} \times ey_{i'}) \times \left(f_{i'}(x_f, t+\Delta t) - f_{i'}^{\text{eq}}(x_f, t+\Delta t)\right) \\ & - \left(g_{i'}(x_f, t) - g_{i'}^{\text{eq}}(x_f, t)\right) \end{aligned} \tag{30}$$

4. Results

In this section, the simulation results are presented and discussed in two parts: in the first part, the heat transfer rate at all points of the isothermal square unit is investigated and compared by presenting the Nusselt number, and in the second part, the temperature field pattern around each cylinder and behind their square unit is studied by isotherms and temperature contours. The mentioned results are reported at Reynolds numbers of 80, 120 and 200. Generally, the heat transfer characteristics of the two upstream cylinders are very close to each other. Likewise, data associated with downstream cylinders are very alike. Accordingly, in the following discussion only one set of data is presented for both cylinders of each column.

4.1. Nusselt number

The heat transfer rate at each point on the surface of cylinders is significantly affected by vortex shedding phenomenon and periodically changes with time with an inconstant period of T_{Nu}. In this simulation, the mentioned inconstant period was used as a gauge to check whether a stable periodic condition was reached or not. In fact, the calculation continued while the change of the mentioned inconstant period T_{Nu} became less than five percents. This means that a stable periodically condition exists. After this condition, the local Nusselt number was computed during thirty other cycles. The time average of local Nusselt number over the last 30 cycles after stable condition is illustrated in Fig. 5. It was checked that involving more cycles makes no significant difference in the accuracy of the results. The panels (a) and (b) show the results for the upstream and downstream cylinders respectively. In this figure, the results of the current simulation are compared with those obtained by Buyruk [25] through finite element solution of the Navier–Stokes and energy equations. As can be seen, there is an excellent agreement between data produced by the LB approach applied in the current study with those reported by Buyruk [25]. The greatest difference between them happens near the stagnation point of cylinders. In the worst cases which are related to Reynolds number of 200, this difference increases to about 8 and 4% for upstream and downstream cylinders, respectively. However, in most points the results are exactly in accordance with each other. It is observed that by

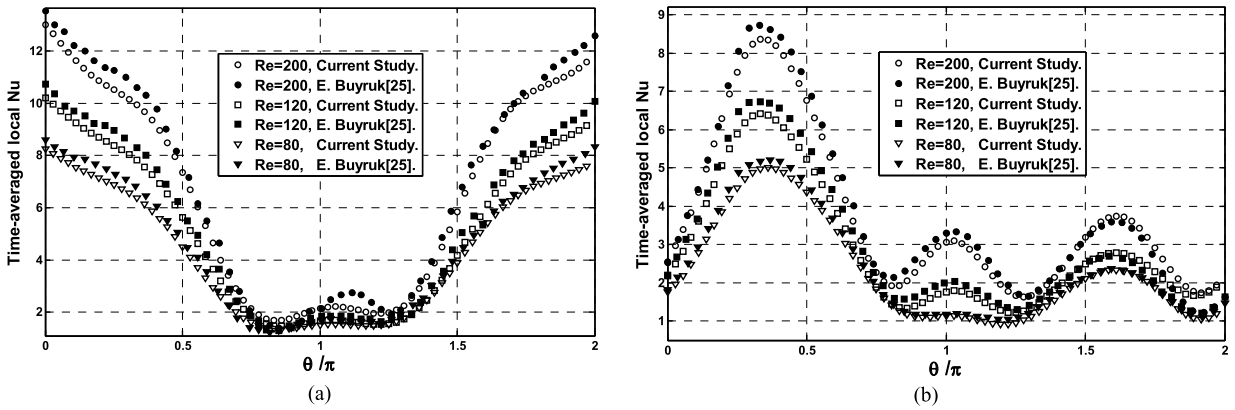

Fig. 5. Panel (a): local Nusselt number of the first column cylinders, panel (b): local Nusselt number of the second column cylinders.

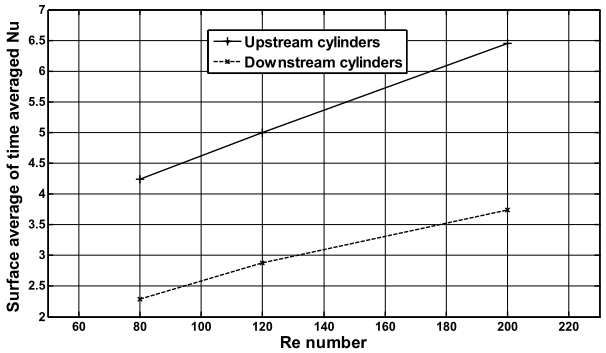

Fig. 6. Mean Nusselt number versus Reynolds number for first and second column cylinders.

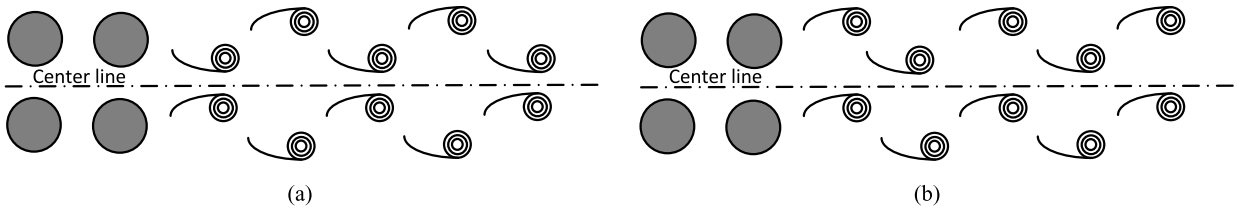

Fig. 7. Schematic of (a) anti-phase and (b) in-phase modes of synchronized vortex shedding.

increase of the Reynolds number, the local Nusselt number on the surface of all cylinders increases. The maximum Nusselt number of each cylinder occurs at the stagnation point. At a fixed Reynolds number, comparing the maximum magnitude of panels (a) and (b) reveals that the local rate of heat transfer at the upstream cylinder stagnation point is significantly higher than those related to downstream cylinders. This is attributed to effect of the wakes of the upstream cylinders which prevent the incoming flow to directly attack the downstream cylinders surfaces.

The surface averages of the local Nusselt numbers presented in Fig. 5 are shown in Fig. 6. According to this figure, surface-averaged Nusselt number of the upstream cylinders is higher in comparison with downstream one. It is found that for the range of Reynolds number chosen in this simulation, there is a linear relation between Reynolds number and surface-averaged Nusselt number, however, the surface-averaged Nusselt number of upstream cylinders increases with a higher rate.

4.2. Temperature distribution

The time evolution of the temperature field behind the square unit of cylinders is directly affected by the vortex shedding phenomenon in a way that the instantaneous isotherms pattern associated with a particular moment is very similar to the predominant vorticity pattern related to that particular time. Generally, different vortex shedding patterns can be classified in two groups: in-phase mode and anti-phase mode which are defined through Fig. 7. In the anti-phase mode the vortex wake pattern behind the square unit is perfectly symmetric and actually the center line acts like a flat mirror. However, in the in-phase mode the vortex wake pattern behind each row of cylinders are completely similar so the total wake

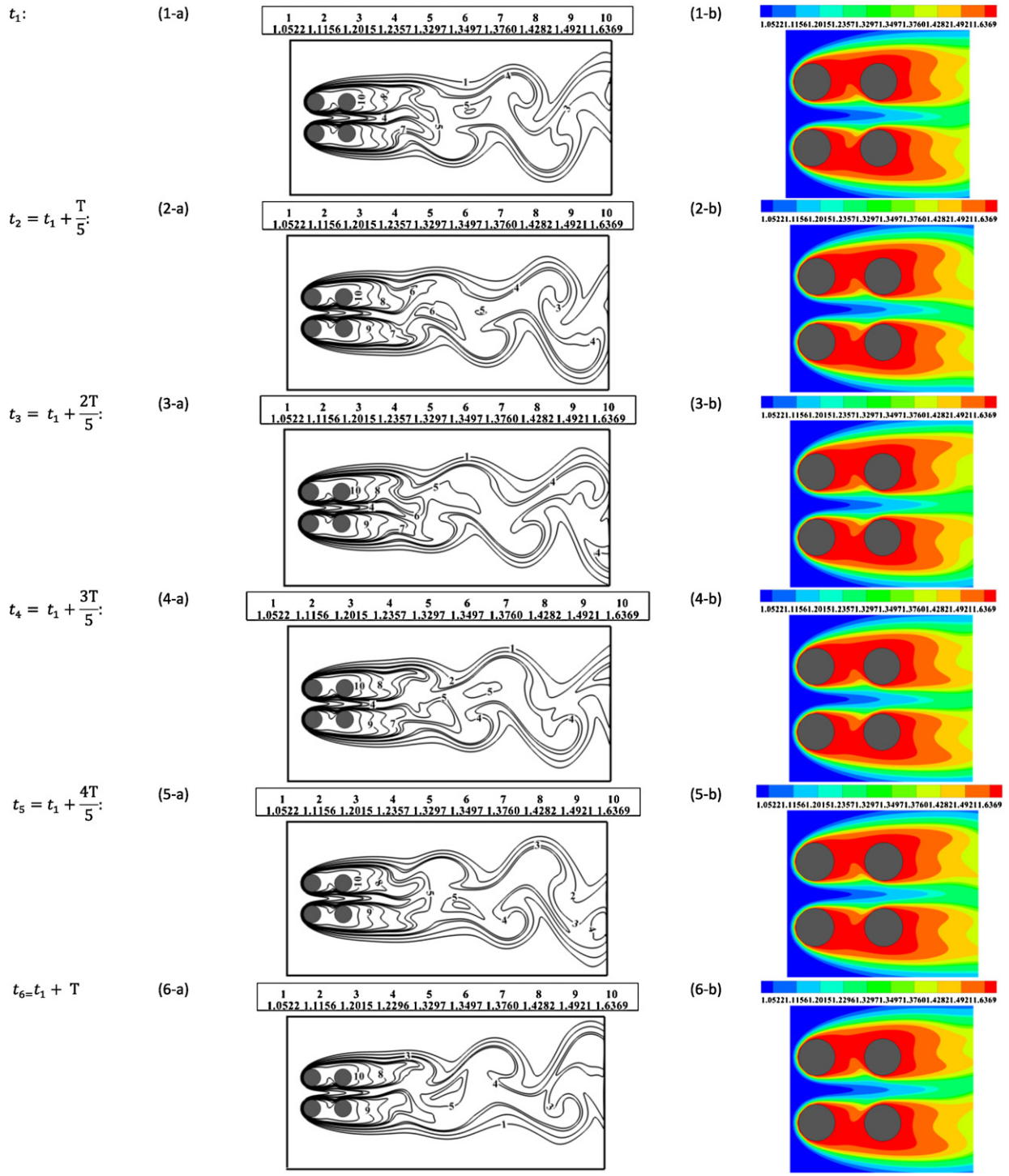

Fig. 8. Panels (a): evolution of the isotherm lines through the whole computational area at Re = 80. Panels (b): thermal shears layer in the near vicinity of cylinders.

pattern is not symmetric. Accordingly, the time evolution of the temperature field can occur in two forms; in-phase time evolution while the vortices shed in the in-phase mode and anti-phase time evolution when anti-phase vortex shedding is the predominant mode.

Fig. 8 comprises two parts: the left column illustrates continuous snapshots of the isotherms through the whole computational domain to study the time evolution of temperature field at Reynolds number of 80, and the right column presents

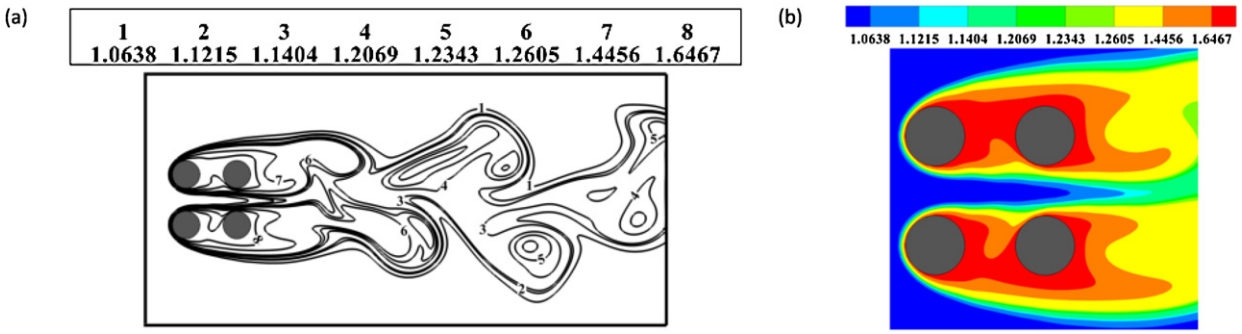

Fig. 9. Panel (a): isotherm lines through the whole computational area at Re = 120. Panel (b): thermal shears layer in the near vicinity of cylinders.

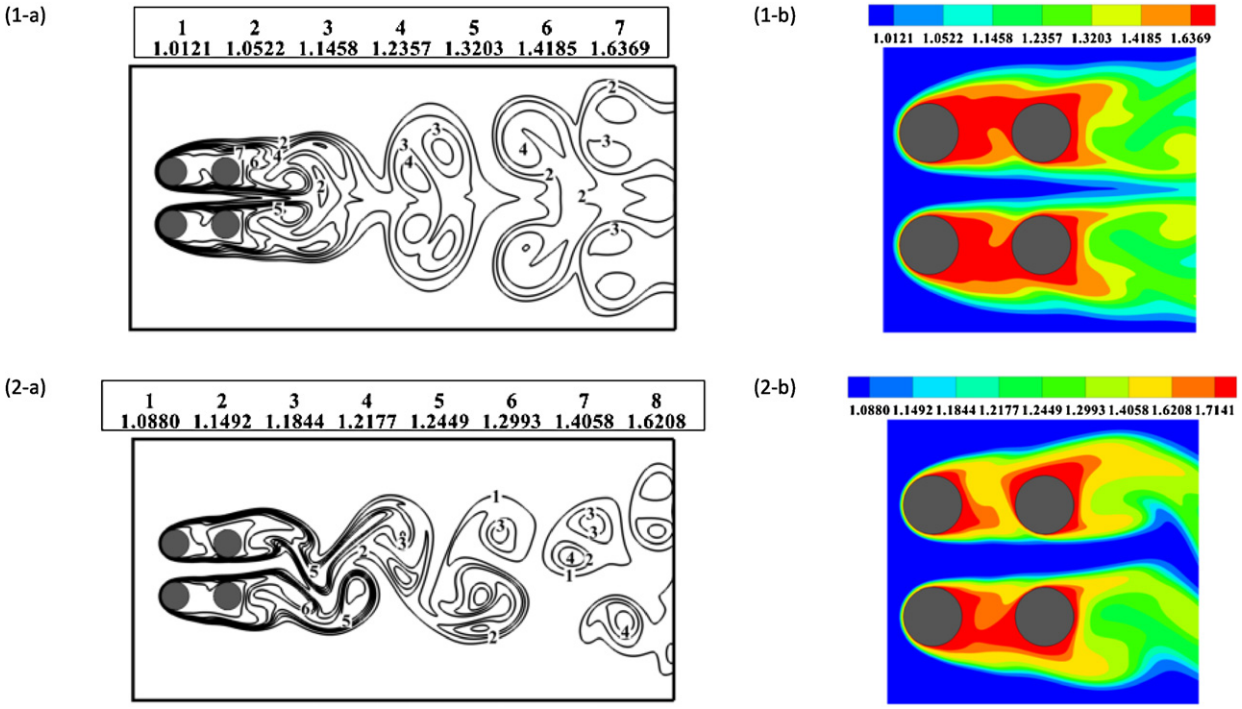

Fig. 10. Panels (1-a) and (2-a): isotherm lines through the whole computational area at Re = 200 in anti-phase and in-phase modes respectively. Panels (1-b) and (2-b): thermal shears layer in the near vicinity of cylinders.

their associated temperature contours. However, these contours are drawn only in the near vicinity of the cylinders to investigate the thermal shear layer treatment. It is clearly seen that at Reynolds number of 80 the time evolution of isotherms occurs in the in-phase mode. Other point which is found from this figure is the fact that during the evolution of the temperature field, the shape of thermal shear layer of both up and down rows of cylinders appears almost constant and also symmetric. As well, it was observed that the temperature field of flow with Reynolds number of 120 constantly evolves in the in-phase mode. Fig. 9 illustrates one snapshot of the mentioned evolution. It is clearly seen that by increasing the Reynolds number the thermal shear layer thickness decreases.

When the Reynolds number increases to 200, both anti-phase and in-phase evolutions are found during the computations, however, at first the anti-phase mode is dominated for a long time. Then the evolution switches to in-phase mode but after a relatively short period of time again the anti-phase mode is observed. After that the temperature field evolution is flipping between these modes alternatively. Panels (1-a) and (2-a) of Fig. 10 present one snapshot from the anti-phase and in-phase modes respectively.

5. Conclusion

In this research the heat transfer characteristic of the flow around a square unit of four isothermal cylinders was investigated using the lattice Boltzmann approach, and the results were presented with Nusselt number and temperature field

contours. It was shown that these results were in accordance with results obtained by finite element solution of Navier–Stokes and energy equation, reported by Buyruk [25].

In conclusion, some of the main points are briefly remarked:

I. The maximum rate of heat transfer of the square unit is related to stagnation point of the upstream cylinder;
II. The mean Nusselt number of upstream cylinders is higher in comparison with the downstream cylinder;
III. Generally, the temperature field evolves in two form; in-phase and anti-phase modes. For the Reynolds numbers of 80 and 120 the evolution only occurs in the in-phase mode, however, at Reynolds number of 200 both modes are observed;
IV. By increasing the Reynolds number, the thermal shear layer thickness of all cylinders decrease.

Acknowledgements

This work was supported by office of the vice chancellor for research, Ferdowsi university of Mashhad, grant 254/4.3.1389.

References

[1] Y. Li, R. Zhang, R. Shock, Prediction of vortex shedding from a circular cylinder using a volumetric lattice-Boltzmann boundary approach, European Physical Journal Special Topics 171 (2009) 91–97.
[2] A. Dupuis, P. Chatelain, P. Koumoutsakos, An immersed boundary–lattice-Boltzmann method for the simulation of the flow past an impulsively started cylinder, Journal of Computational Physics 227 (2008) 4486–4498.
[3] Y. Xia, D.T. Lu, Y. Liu, Y.S. Xu, Lattice Boltzmann simulation of the cross flow over a cantilevered and longitudinally vibrating circular cylinder, Chinese Physics Letters 26 (2009) 034702 (4 pp.).
[4] S. Ul-Islam, C.Y. Zhou, Characteristics of flow past a square cylinder using the lattice Boltzmann method, Information Technology Journal 8 (2009) 1094–1114.
[5] A. Mussa, P. Asinari, L.S. Luo, Lattice Boltzmann simulations of 2D laminar flows past two tandem cylinders, Journal of Computational Physics 228 (2009) 983–999.
[6] Y. Xu, Y. Liu, Y. Xia, F. Wu, Lattice-Boltzmann simulation of two dimensional flow over two vibrating side-by-side circular cylinders, Physical Review E 78 (2008) 046314 (12 pp.).
[7] H. Nemati, K. Sedighi, M. Farhadi, P.M. Mohammadi, E. Fattahi, Numerical simulation of fluid flow of two rotating side-by-side circular cylinders by lattice Boltzmann method, International Journal of Computational Fluid Dynamics 24 (2010) 83–94.
[8] Y. Rao, Y. Ni, C. Liu, Flow effect around two square cylinders arranged side by side using lattice Boltzmann method, International Journal of Modern Physics C 19 (2008) 1683–1694.
[9] S.R. Kumar, A. Sharma, A. Agrawal, Simulation of flow around a row of square cylinders, Journal of Fluid Mechanics 606 (2008) 369–397.
[10] J.A. Esfahani, A.R. Vasel-Be-Hagh, A lattice Boltzmann simulation of cross-flow around four cylinders in a square arrangement, in: ASME 10th Biennial Conference on Engineering Systems Design and Analysis, 2010, p. 24628 (7 pp.).
[11] C.K. Chen, T.S. Yen, Y.T. Yang, Lattice Boltzmann method simulation of a cylinder in the backward-facing step flow with the field synergy principle, International Journal of Thermal Sciences 45 (2006) 982–989.
[12] Y.Q. Zu, Y.Y. Yan, W.P. Shi, L.Q. Ren, Numerical method of lattice Boltzmann simulation for flow past a rotating circular cylinder with heat transfer, International Journal of Numerical Methods for Heat & Fluid Flow 18 (2008) 766–782.
[13] Y.Y. Yan, Y.Q. Zu, Numerical simulation of heat transfer and fluid flow past a rotating isothermal cylinder – A LBM approach, International Journal of Heat and Mass Transfer 51 (2008) 2519–2536.
[14] T.H. Yen, J.K. Kuo, Y.T. Yang, Comparison of heat transfer coefficient in the backward-facing step flow with the LBM and field synergy principle, Journal of the Chinese Society of Mechanical Engineers 30 (2009) 125–134.
[15] L. Djenidi, R.A. Antonia, Momentum and heat transport in a three-dimensional transitional wake of a heated square cylinder, Journal of Fluid Mechanics 640 (2009) 109–129.
[16] Y.T. Yang, C.K. Chen, S.C. Chang, S.Y. Sun, LBM simulations of channel flow with a cylinder by the field synergy principle, Progress in Computational Fluid Dynamics 9 (2009).
[17] M. Moussaoui, M. Jami, A. Mezrhab, H. Naji, Convective heat transfer over two blocks arbitrary located in a 2D plane channel using a hybrid lattice Boltzmann-finite difference method, Heat Mass Transfer 45 (2009) 1373–1381.
[18] X.Y. Kang, X. Zhu, Q. Liao, Simulation of fluid flow and heat transfer around a cylinder by lattice Boltzmann method, Huaxue Gongcheng/Chemical Engineering (China) 30 (2010) 21–24.
[19] J. Ghasemi, S.E. Razavi, On the finite-volume lattice Boltzmann modeling of thermo-hydrodynamics, Computers and Mathematics with Applications 60 (2010) 1135–1144.
[20] M. Moussaoui, M. Jami, A. Mezrhab, H. Naji, MRT-lattice Boltzmann simulation of forced convection in a plane channel with an inclined square cylinder, International Journal of Thermal Sciences 49 (2010) 131–142.
[21] M. Sukop, D. Thorne, Lattice Boltzmann Modeling: An Introduction for Geoscientists and Engineers, Springer-Verlag, Berlin, Heidelberg, 2006.
[22] M. Sukop, D. Or, Invasion percolation of single component, multiphase fluids with lattice Boltzmann models, Physica B 338 (2003) 298–303.
[23] Z. Guo, C. Zheng, An extrapolation method for boundary conditions in lattice Boltzmann method, Physics of Fluids (2002), http://dx.doi.org/10.1063/1.1471914.
[24] Q. Zou, X. He, On pressure and velocity boundary conditions for the lattice Boltzmann BGK model, Physics of Fluids 9 (1997) 1591–1598.
[25] E. Buyruk, Numerical study of heat transfer characteristics on tandem cylinders, in-line and staggered tube banks in cross flow of air, International Communications in Heat and Mass Transfer 29 (2002) 355–366.